Graefes Arch Clin Exp Ophthalmol (2015) 253:1591–1600
DOI 10.1007/s00417-015-2979-1

NEUROPHTHALMOLOGY

# Multifocal VEP provide electrophysiological evidence of predominant dysfunction of the optic nerve fibers derived from the central retina in Leber's hereditary optic neuropathy

**Lucia Ziccardi · Vincenzo Parisi · Daniela Giannini · Federico Sadun · Anna Maria De Negri · Piero Barboni · Chiara La Morgia · Alfedo A. Sadun · Valerio Carelli**

Received: 5 December 2014 / Revised: 26 February 2015 / Accepted: 27 February 2015 / Published online: 17 March 2015


**Abstract**
*Purpose* To differentiate the bioelectrical cortical responses driven by axons from central and mid-peripheral retina in Leber's hereditary optic neuropathy (LHON) by using multifocal visual evoked potentials (mfVEP).
*Methods* Seventeen genetically confirmed LHON patients (33.35±8.4 years, 17 eyes) and 22 age-matched controls (C) (38.2±6.0 years, 22 eyes) were studied by mfVEP and optical coherence tomography. MfVEP P1 implicit time (P1 IT, ms) and response amplitude density of the N1-P1 components (N1-P1 RAD, nV/deg$^2$) of the second order binary kernel were measured for five concentric retinal areas between the fovea and mid-periphery: 0–20 degrees (R1 to R5).
*Results* Mean mfVEP P1 ITs and N1-P1 RADs at all five foveal eccentricities were significantly different ($p<0.01$) in LHON when compared to controls. In both groups, mean mfVEP responses obtained from R1 to R5 showed a progressive shortening of P1 ITs (linear fitting, LHON: $r=-0.95$; C: $r=-0.98$) and decrease of N1-P1 RADs (exponential fitting, LHON: $r^2=0.94$; C: $r^2=0.93$). The slope of the linear fitting between mean mfVEP P1 ITs in the two groups was about three times greater in LHON than in controls (LHON: y= −13.33x +182.03; C: y=−4.528x +108.1). MfVEP P1 ITs detected in R1 and R2 (0–5 degrees) were significantly correlated ($p<0.01$) with the reduction of retinal nerve fiber layer thickness of the temporal quadrant.
*Conclusions* MfVEP identifies abnormal neural conduction along the visual pathways in LHON, discriminating a predominant involvement of axons driving responses from the central retina when compared to those serving the mid-peripheral retina.

L. Ziccardi (✉) · V. Parisi
Neurophthalmology Unit, Fondazione G.B. Bietti- IRCCS, Via Livenza 3, 00198 Rome, Italy
e-mail: luxzic@hotmail.com

D. Giannini
Department of Statistical Sciences, "La Sapienza" University, Piazzale Aldo Moro 5, 00185 Rome, Italy

F. Sadun
Ospedale San Giovanni Evangelista, Via Parrozzani 3, 00019 Tivoli, Italy

A. M. De Negri
Azienda San Camillo-Forlanini, Circonvallazione Gianicolense 87, 00152 Rome, Italy

P. Barboni
Studio oculistico d'Azeglio, Via D'Azeglio 5, 40123 Bologna, Italy

P. Barboni
IRCCS Istituto Scientifico San Raffaele, Via Olgettina 60, 20132 Milan, Italy

C. La Morgia · V. Carelli
Bellaria Hospital, IRCCS Istituto delle Scienze Neurologiche di Bologna, Via Altura 3, 40139 Bologna, Italy

C. La Morgia · V. Carelli
Dipartimento di Scienze Biomediche e Neuromotorie (DIBINEM), Neurology Unit, University of Bologna, Via Ugo Foscolo 7, 40123 Bologna, Italy

A. A. Sadun
Doheny Eye Institute, UCLA, 1450 San Pablo St, Los Angeles, CA 90033, USA

**Keywords** Multifocal visual evoked potentials · Leber's hereditary optic neuropathy · LHON · Retinal ganglion cells function · Mitochondrial optic neuropathy

## Introduction

Multifocal visual evoked potentials (mfVEP) is a tool commonly used to assess retino-cortical processing, in order to characterize functional impairment at the post ganglion cell level [1], allowing the detection of pathologies of the visual pathways involving localized field losses [2–4].

Based on the method of presenting pseudo-random multifocal stimulations together with cortical scaling of the stimulated patches' size, the mfVEP system allows the simultaneous stimulation of numerous locations of the visual field, and can extract individual responses from each of them. Thus, because of its ability to stimulate a large number of receptive fields simultaneously and independently, this method records responses from many locations of the visual field that enable the studying of visual field topography of the cortical responses [5, 6]. In the evaluation of the whole mfVEP response, it is known that by using the cross-correlation as a function of visual stimuli located in concentric retinal areas at different eccentricity from the fovea, it is possible to obtain bioelectrical responses from 0–2.5, 2.5–5, 5–10, 10–15 and 15–20 degrees of the retina [4, 7]. This method, known as "ring analysis", permits the discrimination of the contribution of axons driving responses from the central retina from that of the more peripheral retinal areas [4, 7].

Leber's hereditary optic neuropathy (LHON) is a mitochondrial disorder characterized by bilateral acute/sub-acute loss of central vision (acute phase) and with subsequent variable degrees of optic nerve atrophy (chronic phase) [8]. Three mitochondrial DNA point mutations affecting complex I of the respiratory chain (11778G>A/ND4, 3460G>A/ND1 and 14484T>C/ND6) have been described as pathogenic for LHON, and account for almost 95 % of cases [9]. In the acute phase of LHON, there is an early and selective involvement of the central retina and specifically of the papillo-macular bundle (PMB), which rapidly progresses to axonal loss in the temporal sector, responsible for the sudden loss of central vision with cecocentral scotoma. In the chronic phase of the disease, patients develop pallor of the optic disc that is more marked on the temporal side, thus indicating various degrees and extension of optic atrophy [10].

The aim of this study was to investigate the capability of multifocal visual evoked potentials to differentiate the bioelectrical cortical responses driven by axons from central and peripheral retinal areas in Leber's hereditary optic neuropathy.

## Materials and methods

### Patients

Enrolled in the study were seventeen eyes from 17 affected LHON patients (age ranging from 20 to 45 years, mean age 32.2±9 years) having a molecularly confirmed diagnosis of LHON because of harboring either the 11778/ND4 (10/17), or the 3460/ND1 (5/17) or the 14484/ND6 (2/17) mutation. LHON patients belonged to nine different pedigrees. Twenty-two eyes from 22 normal age-similar subjects (mean age 38.2±6.0 years, range: 19–48 years) served as controls.

All subjects underwent extensive ophthalmologic characterization, including best-corrected visual acuity (BCVA) measurement with the Early Treatment Diabetic Retinopathy Study (ETDRS) charts, expressed as a logarithm of the minimum angle of resolution (logMAR), slit-lamp biomicroscopy, intraocular pressure (IOP) measurement, indirect ophthalmoscopy, optic nerve head 30° color standard photography, and Humphrey 24–2 automated visual field test (HFA), optical coherence tomography (OCT), and mfVEP.

Normal subjects had an intraocular pressure less than 18 mmHg, BCVA of 0.0 logMAR with a refractive error between −2.00 and +2.00 spherical equivalent, HFA 24–2 with a mean deviation (MD) of ±0.5 dB and corrected pattern standard deviation (CPSD) <1 dB, and no evidence of optic disc or retinal disease.

LHON patients had been experiencing the onset of symptoms for 2 years or more (mean duration of disease 32±8 months, ranging from 24 to 40 months), BCVA was between 0.00 and 0.50 logMAR, 24–2 HFA MD was between −2 and −10 dB, CPSD was >2 dB, patients presented one or more papillary signs of LHON on conventional 30° color stereo slides (optic disc pallor, optic disc hyperemia, microangiopathy, peripapillary atrophy), and refractive error (when present) was between −3.00 and +3.00 spherical equivalent; no previous history or presence of any ocular disease involving cornea, lens and retina/ macula, or detectable spontaneous eye movements (i.e., nystagmus) was found. For each LHON patient, the eye with the highest BCVA was selected for the study.

Excluded from the present study were all eyes showing any sign of optic nerve pathology other than LHON and patients with Humphrey visual field centrocecal scotoma that did not allow perceiving the target of the multifocal mVEP stimulation (see below).

All participants gave their informed consent. The research followed the tenets of the Declaration of Helsinki, and the study was approved by the Local Ethics Committee (Azienda Sanitaria Locale Roma A).

## Visual field analysis

Visual fields (VF) (Humphrey Field Analyzer, protocol Sita Standard 24–2; Zeiss, San Leandro, CA, USA) were performed in controls and LHON patients twice in 1 month, and the second examination was considered for the analysis. The MD and CPSD indexes of the VF were recorded. Moreover, in the analysis of tests recorded in LHON patients, we qualitatively assessed the spatial distribution of reduced retinal sensitivity based on the pattern deviation plot. Considering the points of statistically significant field loss at the 0.5 percent level, we classified a loss exclusively located up to 10 degrees as "A", and a loss extending over the 10 degrees as "B".

## Multifocal visual evoked potentials (MfVEP) recording

The mfVEP testing was performed using VERIS Clinic™ 4.9 software (Electro-Diagnostic Imaging, San Mateo, CA, USA) according to our previously published method [4]. The dartboard pattern consisted of 60 sectors, each sector having a checkerboard pattern of 16 checks, eight white (200 cd/m$^2$) and eight black (1 cd/m$^2$). The sectors were cortically scaled with eccentricity to stimulate approximately equal areas of the visual cortex (i.e., central sectors were smaller than peripheral sectors). The entire dartboard subtended an area with a radius of 20 degrees. The stimulus array was displayed on a black-and-white monitor driven at a frame rate of 75 Hz. The 16-element checkerboard of each sector had a probability of 0.5 of reversing on any pair of frame changes and the pattern of reversals for each sector followed a pseudorandom (m-) sequence.

The stimulation was monocular, with full occlusion of the fellow eye. In order to maintain a stable fixation, a small red target (0.5 deg) that was perceived by all subjects tested, was placed in the center of the stimulation field. Prior to the experiment, each subject was adapted to the room light for 10 minutes and the pupil diameter was about 5 mm. Mydriatic or miotic drugs were never used. MfVEP were recorded by cup shaped Ag/AgCl electrodes placed 4 cm above the inion (active), at the inion (reference), and on the forehead (ground). The interelectrode resistance was kept below 3 kΩ. VEP signals were amplified (gain 20,000), filtered (bandpass 1-100Hz, −6 dB/octave), and sampled with 12-bit resolution (BM6000, Biomedica Mangoni, Pisa, Italy). Each recording session was subdivided into 14 recording segments of approximately 60s duration. The total duration of a recording session was about 14 min. The VERIS Scientific software™ (VERIS software, EDI, San Mateo, CA, USA) was used to calculate the 60 local VEP responses from the measured signal and to analyze the second order kernels. A typical waveform begins with a negative deflection (N1), followed by a positive deflection (P1) and a second negative deflection (N2). To analyze the mfVEP amplitudes, we calculated the response amplitude density (nanoVolt/degree $^2$, nV/deg$^2$) between N1 and P1 peaks; to analyze the mfVEP implicit time (in milliseconds, ms), we restricted the analysis to timing of the first positive deflection (P1).

### *Signal-to-noise ratio*

MfVEP signal-to-noise ratio (SNR) was estimated following the methodology discussed by Hood and Greenstein [2]. Briefly, a noise window was set as part of the record such that the recording was of equal length to the period within which the response was analysed, but it was included in a temporal window that was assumed to contain little or no response. For the mfVEP, the signal temporal window was 0–200 ms, while the noise temporal window was 200–400 ms [4]. SNR was defined as the ratio of root mean square (RMS) signal plus noise (measured in the signal temporal window) of a given record to the mean RMS of all noise windows (60 for the mfVEP). A SNR of ≥3 was accepted for mfVEP measurements. A "recordable" response had to have a SNR≥3.

### *Ring analysis*

In order to evaluate cortical responses related to the stimulation of annular retinal areas between the fovea to mid-periphery, ring analysis was performed for mfVEP P1 implicit time (P1 IT, ms) and response amplitude density of the N1-P1 components (N1-P1 RAD, nV/deg$^2$) of the second order binary kernel measured in response to visual stimuli presented on five retinal areas between the fovea and mid-periphery, with a radius of 0–2.5 (ring 1, R1), 2.5–5 (ring 2, R2), 5–10 (ring 3, R3), 10–15 (ring 4, R4), and 15–20 (ring 5, R5) degrees.

## Optical coherence tomography analysis

In controls and LHON eyes, the peripapillary retinal nerve fiber layer (RNFL) thickness was assessed by spectral domain OCT (RTVue Model-RT100 version 3.5; Optovue Inc, Fremont, CA, USA).

Peripapillary RNFL 3.45 protocol was used. This system provides the operator with a video-camera view of the scanning probe beam on the fundus, and OCT imaging acquired in real time on a computer monitor. After dilatation with 1 % tropicamide, each eye was scanned three times using a circle size of 3.4 mm (1.7 mm radius). Throughout scanning, the patient kept his/her eyes constantly fixed on an internal target provided by the equipment. The measurements were obtained from three non-consecutive scans (i.e., the patient was allowed to rest for a few seconds before being re-positioned to proceed to the following scan). The software allows the mapping of the thickness data according to both quadrant-by-quadrant and clock hour analyses. RNFL thickness was determined by computer as the distance between the first reflection at the vitreoretinal interface and the anterior boundary of the second reflective layer, corresponding to the retinal

pigment epithelium and the choriocapillaris. We considered the average value of four different measurements per quadrant (RNFL superior, inferior, nasal and temporal); the overall data obtained in all quadrants (16 values averaged) was identified as RNFL Overall.

### Statistics

We assumed a Gaussian distribution of our data. The normal distribution was tested by using the Kolmogorov–Smirnov test. For all electrophysiological and OCT parameters, 95 % confidence limits were obtained from age-similar normal subject data by calculating mean values minus and plus 2 standard deviations (SD): mean values plus 2 standard deviations were calculated for mfVEP P1 ITs (upper limit), and mean values minus 2 standard deviations for mfVEP RADs and RNFL thickness (lower limit). Only one eye, the one having the highest BCVA, was evaluated for each subject. Differences of electrofunctional parameters (mfVEP R1-R5 N1-P1 RADs and P1 ITs) between control and LHON groups and within the LHON group (LHON "A" and "B" eyes, see below) were evaluated by one-way analysis of variance (ANOVA). Linear and exponential fittings were applied to describe the progression of the mfVEP RADs and P1 ITs values across rings from 1 to 5. Pearson's correlation was used in order to examine possible association between mfVEP IT data and RNFL thickness. For all analyses, a conservative $p$-value of <0.01, compensating for multiple correlations, was considered as statistically significant. SAS statistical software package (version 9.1, SAS Institute Inc, Cary, NC, USA) was used.

## Results

### Multifocal VEP results

Figure 1 shows examples of mfVEP recordings from a control eye and from a representative LHON eye (L#11 of Tables 1 and 2) (a) with corresponding VF (b and c) and RNFL thickness (d).

Table 1 shows the mfVEP P1 IT individual outcomes detected in LHON eyes with respect to our normal limits. All (17/17) LHON eyes presented abnormal values in the more central rings: ring 1 and ring 2. In the more peripheral rings (R3, R4, and R5), we found abnormal values for mfVEP P1 ITs in the majority of LHON eyes: 16/17, 12/17, and 14/17 eyes respectively. In the same table is reported the qualitative

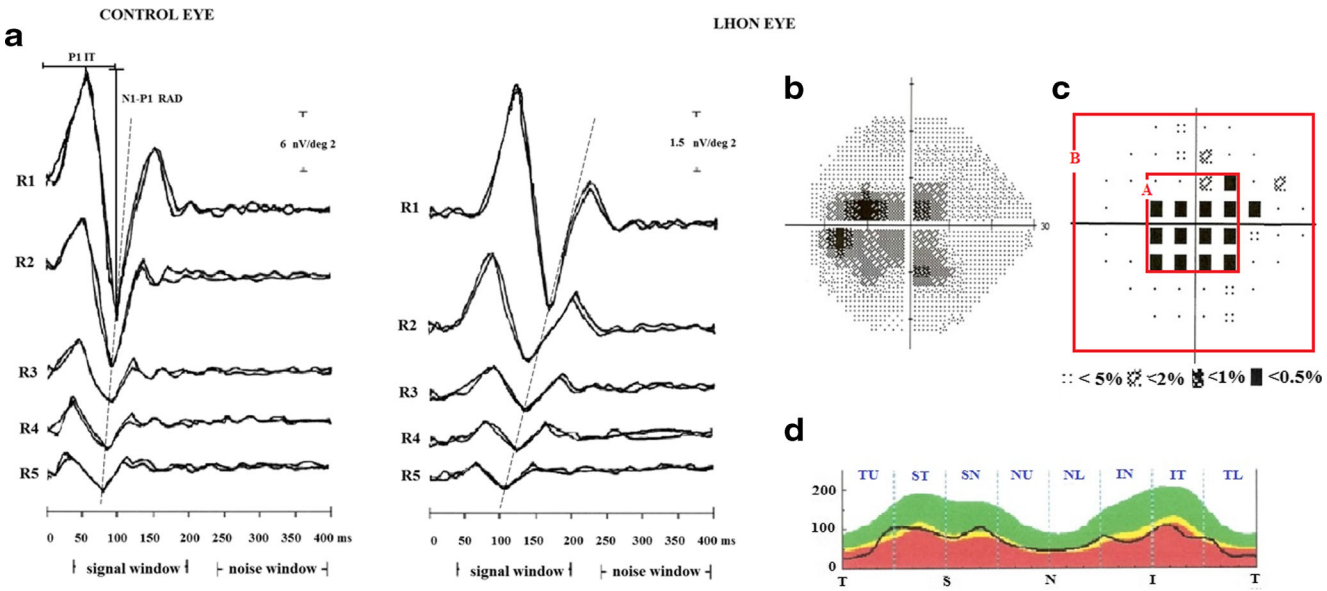


**Fig. 1** **a** Layout of multifocal visual evoked potentials (mfVEP) second order response components recorded in one control eye and in one representative eye affected by Leber's hereditary optic neuropathy (LHON, L#11). MfVEP local responses were averaged in five retinal areas located at various degrees of eccentricity from the fovea: 0–2.5 (ring 1: R1), 2.5–5 (ring 2: R2), 5–10 (ring 3: R3), 10–15 (ring 4: R4) and 15–20 (ring 5: R5) degrees. IT, implicit time, ms; RAD, response amplitude density, nV/deg$^2$. MfVEP responses obtained from central to peripheral rings (R1 to R5) show a progressive shortening of P1 ITs and decrease of N1-P1 RADs in both control and LHON eyes. The *dashed line* shows this phenomenon in control and LHON eyes, showing a different steepness in the LHON eye than in the control one. **b** Humphrey Field Analyzer visual field tested in L#11 eye, and **c** relative pattern deviation plot, where the *red squares* indicate two areas with increased eccentricity from the center of fixation (0 degrees): 0–10 degrees (*A*), over 10 degrees (*B*), used to assess qualitatively the spatial distribution of reduced retinal sensitivity. In this case, we observed a loss of retinal sensitivity extending over 10 degrees. **d** Peripapillary retinal nerve fiber layer (RNFL) thickness evaluated by optical coherence tomography assessed in eight sectors of the optic nerve scan of L#11 eye (*TU*: temporal–upper, *ST*: superior–temporal, *SN*: superior–nasal, *NU*: nasal–upper, *NL*: nasal–lower, *IN*: inferior–nasal, *IT*: inferior–temporal, and *TL*: temporal–lower). For L#11 eye, the mfVEP, HFA prevalent loss of retinal sensitivity, and OCT values are reported in Tables 1 and 2

**Table 1** Individual multifocal visual evoked potentials (mfVEP) P1 implicit time (IT, milliseconds) values recorded in Leber's hereditary optic neuropathy (L) patients

| | R1 P1 IT (ms) | R2 P1 IT (ms) | R3 P1 IT (ms) | R4 P1 IT (ms) | R5 P1 IT (ms) | Spatial distribution of retinal sensitivity loss |
|---|---|---|---|---|---|---|
| L#1 | 202.4* | 180.8* | 175.8* | 138.3* | 140.8* | B |
| L#2 | 169.9* | 170.8* | 178.3* | 100 | 129.9* | B |
| L#3 | 139.9* | 169.9* | 183.3* | 157.4* | 144.1* | B |
| L#4 | 134.1* | 140.8* | 143.3* | 81.6 | 71.6 | A |
| L#5 | 163.3* | 179.1* | 175.8* | 125.8* | 144.1* | B |
| L#6 | 206.6* | 219.9* | 200.7* | 145.8* | 124.9* | B |
| L#7 | 167.4* | 167.4* | 145.8* | 125.8* | 131.6* | B |
| L#8 | 184.9* | 189.9* | 155.8* | 111.6* | 112.5* | A |
| L#9 | 143.3* | 144.1* | 135.8* | 119.1* | 109.1* | A |
| L#10 | 177.4* | 139.1* | 138.3* | 143.3* | 141.6* | B |
| L#11 | 167.4* | 134.9* | 134.9* | 122.4* | 105.8* | B |
| L#12 | 132.4* | 119.1* | 115.8* | 110* | 109.1* | A |
| L#13 | 172.4* | 151.6* | 144.9* | 106.6* | 103.3* | A |
| L#14 | 196.6* | 194.9* | 196.6* | 119.1* | 119.9* | B |
| L#15 | 139.1* | 147.4* | 94.1 | 98.3 | 102.5* | A |
| L#16 | 167.4* | 160.8* | 143.3* | 100.8 | 98.3 | A |
| L#17 | 132.4* | 131.6* | 120.8* | 98.3 | 89.1 | A |
| 95 % CL | | | | | | |
| U | 114.3 | 107.2 | 105.72 | 101.41 | 102 | |

R1–R5 refers to five concentric annular retinal regions (rings) centered on the fovea: R1: 0–2.5 degrees; R2: 2.5–5 degrees; R3:5–10 degrees; R4: 10–15 degrees; R5: 15–20 degrees. 95 % confidence limits (CL). Normal limits obtained from control subjects by calculating mean values plus 2 standard deviations (upper limit U). *Values are outside the normal limits. The last column displays the spatial distribution of the points with statistically significant field loss at the 0.5 percent level of the Humphrey Field Analyzer pattern deviation plot. "A" refers to the visual field areas with an exclusive loss localized into 10 degrees, "B" refers to a loss extending over 10 degrees

analysis of the spatial distribution of the retinal sensitivity loss. In LHON eyes, we observed an exclusive loss within the 10 degrees in 8/17 eyes (eight "A" eyes), a loss extending over the 10 degrees in 9/17 eyes (nine "B" eyes).

Figure 2 features individual mfVEP IT values from LHON eyes plotted against correspondent foveal eccentricities (from 0 to 20 degrees). It can be noted that by proceeding with increased eccentricities, all LHON mfVEP IT measurements (represented by dashed lines) from the more central rings (R1 to R2) were prolonged with respect to the upper 95 % confidence limit of control eyes (represented by a solid line), whereas the distribution of LHON individual outcomes from the more peripheral rings (R3 to R5) was such that some values fell below the upper 95 % normal confidence limit.

Table 2 shows the mfVEP N1-P1 RAD individual values found in LHON eyes. Twelve out of 17 LHON eyes presented values outside the lower 95 % confidence limit in ring 1 and in ring 4; all but one value were abnormal in ring 2; 10/17 LHON eyes had abnormal values in ring 3, and all eyes presented amplitude values in the 95 % confidence limit in ring 5.

On average, significant ($p<0.01$) differences were found at all five eccentricities, in both mfVEP P1 ITs and in N1-P1 RADs when comparing control and LHON eyes (Table 3).

On the basis of the data reported in Table 1, it is possible to observe that when in LHON eyes the retinal sensitivity loss was located exclusively into the 10 degrees (LHON "A" eyes), individual mfVEP P1 ITs derived from the more external rings (R4 and R5) were within the normal limits (four of eight LHON "A" eyes) or were delayed (four of eight LHON "A" eyes) with respect to our normal limits, whereas all LHON eyes with a loss extending over the 10 degrees (nine of nine LHON "B" eyes) showed abnormal P1 IT values. On average, significant differences ($p<0.01$) of mfVEP P1 ITs between LHON "A" and "B" eyes were found in the more external rings (R3 to R5) (Table 3). Meanwhile, not significant differences ($p>0.01$) between the two LHON groups were found at all eccentricities for mfVEP N1-P1RADs and in the central rings (R1 and R2) for mfVEP P1 ITs.

In Fig. 3a and b, mean values of mfVEP P1 IT and N1-P1 RAD respectively recorded in control and LHON eyes are plotted as a function of retinal eccentricity (0–20 degrees). In both control and LHON eyes, mean mfVEP responses obtained from R1 to R5 showed a progressive shortening of P1 ITs (Fig. 3a: linear fitting, LHON: $r=-0.95$; Controls: $r=-0.98$) and decrease of N1-P1 RADs (Fig. 3b: exponential fitting, LHON: $r^2=0.94$; Controls: $r^2=0.93$). However, the slope of the function describing the progression of mean

**Table 2** Individual values of multifocal visual evoked potentials (mfVEP) N1-P1 response amplitude density (RAD, nanovolt/degree$^2$) and retinal nerve fiber layer (RNFL) overall and temporal thickness (microns) measured by optical coherence tomography (OCT) in Leber's hereditary optic neuropathy (L) patients

| | R1 N1-P1 RADs (ηV/deg$^2$) | R2 N1-P1 RADs (ηV/deg$^2$) | R3 N1-P1 RADs (ηV/deg$^2$) | R4 N1-P1 RADs (ηV/deg$^2$) | R5 N1-P1 RADs (ηV/deg$^2$) | RNFL OCT overall thickness (microns) | RNFL OCT temporal thickness (microns) |
|---|---|---|---|---|---|---|---|
| L#1 | 26.8 | 4.4* | 1.5 | 1.4* | 0.9 | 56.79* | 32.5* |
| L#2 | 38 | 3.6* | 2.4 | 1.3* | 0.3 | 64.35* | 49* |
| L#3 | 8.4* | 4* | 1.6 | 0.9* | 0.4 | 88.6* | 53.75* |
| L#4 | 16.1* | 0.8* | 0.7* | 0.2* | 0.5 | 90.6* | 46.5* |
| L#5 | 12.7* | 2.5* | 1.9 | 1.1* | 0.9 | 66.24* | 37.75* |
| L#6 | 10.4* | 7.6* | 1* | 0.9* | 0.8 | 59.74* | 32.25* |
| L#7 | 8* | 2.8* | 1* | 0.4* | 0.5 | 55.8* | 29.5* |
| L#8 | 38 | 6.6* | 2.5 | 0.8* | 0.3 | 70* | 25.25* |
| L#9 | 8.4* | 2.5* | 0.8* | 0.5* | 0.2 | 58.78* | 50* |
| L#10 | 4.2* | 1.5* | 1* | 0.4* | 0.2 | 64.64* | 50* |
| L#11 | 5.7* | 2.8* | 1.2* | 0.7* | 0.7 | 66.91* | 46* |
| L#12 | 8.7* | 1.5* | 0.5* | 0.3* | 0.2 | 75.72* | 45* |
| L#13 | 5* | 3.4* | 0.6* | 0.1* | 0.2 | 89.05* | 52* |
| L#14 | 12.8* | 1.3* | 0.8* | 0.4* | 0.3 | 72.49* | 33* |
| L#15 | 12.2* | 4.5* | 1* | 1.1* | 0.3 | 78.06* | 55* |
| L#16 | 20.5 | 9.3 | 1.3 | 0.8* | 0.2 | 82.25* | 52.25* |
| L#17 | 26.3 | 7* | 1.8 | 1.3* | 0.8 | 76.4* | 56* |
| 95 % CL | | | | | | | |
| L | 18.26 | 9.09 | 1.24 | 1.7 | 0.08 | 92.28 | 60.94 |

R1–R5 refers to five concentric annular retinal regions (rings) centered on the fovea: R1: 0–2.5 degrees; R2: 2.5–5 degrees; R3:5–10 degrees; R4: 10–15 degrees; R5: 15–20 degrees. 95 % confidence limits (CL). Normal limits obtained from control subjects by calculating mean values minus 2 standard deviations (lower limit L). *Values are outside the normal limits

mfVEP P1 ITs shortening with increased eccentricity was more than three times greater in LHON than in control eyes (LHON: $y=-13.33x+182.03$; Controls: $y=-4.528x+108.1$). This difference was remarkable when proceeding from R3 to R4, which corresponds to the center–peripheral transitional stimulated retinal areas (center to periphery: 5 to 10 degrees of foveal eccentricity).

In particular, the greatest difference of mean mfVEP ITs between LHON and control eyes was detected in the first three rings (R1 to R3), resulting in more abnormal responses from the more central retinal regions (0–10 degrees from the fovea) than from the more eccentric annular rings (R4 and R5) carrying neural information from the more peripheral retinal regions (10–20 degrees from the fovea) (Figs. 2 and 3a). Similarly, when comparing mean mfVEP N1-P1 RAD values between controls and LHON eyes, we found that the amplitude differences in R1 to R3 were larger than the ones found in R4 and R5 (Fig. 3b).

### RNFL thickness results and correlations with mfVEP findings

Individual LHON values of overall and temporal sector RNFL thickness are reported in Table 2. All LHON eyes presented abnormal values which were outside the lower 95 % confidence limit, derived from control values (mean±SD *O*verall RNFL thickness: 104.80±6.26 microns; *M*ean±SD *T*emporal RNFL thickness: 80.2±9.63 microns).

Table 4 shows the correlations between mfVEP IT and RAD values recorded from ring 1 to ring 5, and the RNFL overall and temporal thickness values from our cohort of LHON eyes. We found statistically significant correlations ($p<0.01$) between the *T*emporal RNFL thickness measurements and mfVEP P1 IT values detected in the central rings (R1 and R2). A trend of correlation, without reaching the level of significance ($p=0.032$), was found in R3. Not significant correlations ($p>0.01$) were found between temporal RNFL values and mfVEP P1 ITs from R4 and R5. Not significant correlations ($p>0.01$) were found also between overall RNFL measurements and R1-R5 mfVEP P1 ITs and RADs.

## Discussion

The aim of this study was to establish whether the mfVEP technique was capable of differentiating the bioelectrical

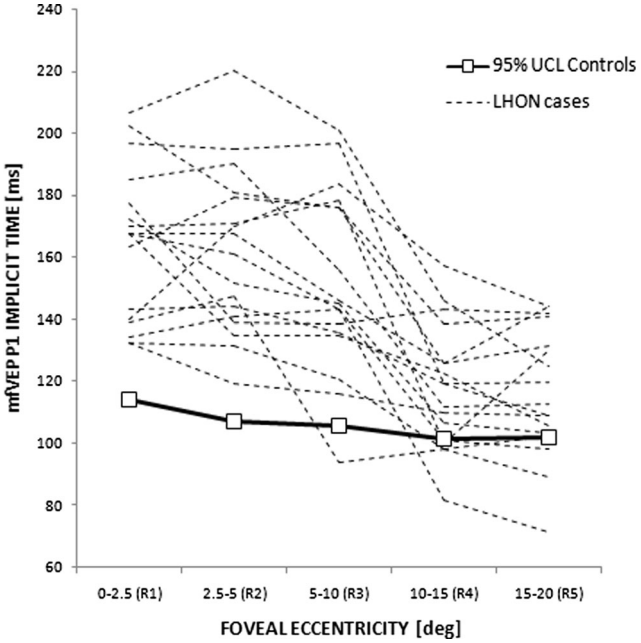


**Fig. 2** Individual multifocal visual evoked potentials (mfVEP) P1 implicit time (IT) values from Leber's hereditary optic neuropathy (LHON) eyes represented by *dashed lines* are plotted as a function of foveal eccentricities. R1 to R5 refer to ring analysis (see Methods). Upper 95 % confidence limit (UCL) for controls is represented by a *solid line*. By proceeding with increased eccentricities, all LHON mfVEP IT measurements from the more central rings (ring 1 to ring 3, 0–10 degrees of eccentricities) are significantly more prolonged than in controls, whereas some of LHON P1 IT individual outcomes from the more peripheral rings (ring 4 and ring 5, 10 to 20 degrees of eccentricities) overlap or fall below the 95 % UCL

cortical responses driven by axons from central and peripheral retinal areas in Leber's hereditary optic neuropathy.

## MfVEP responses in normal subjects

Our electrophysiological outcomes of decreased mfVEP implicit times, as a function of increasing foveal eccentricity, can be explained by the retinal anatomy and neurophysiology of the neural component of the visual pathways in normal eyes. As a consequence of the decreasing ganglion cell/receptor ratio, cell densities have a steeper drop-off with eccentricity, and the receptive field sizes increase with distance from the foveola [11, 12]. Sutter and Bearse [13] pointed out that for each ring of foveal eccentricity there exists a linear relation between axon fiber length and implicit time. Fukuda and co-authors [14] verified that velocities are proportional to the square root of the neural fiber diameter. Thus, the estimated mean propagation velocity of axon fibers deriving from the concentric rings increases with eccentricity from about 40 cm/s at the innermost ring at 2–5° to about 120 cm/s at approximately 12.5–17.5° eccentricity [13]. Fiber diameter distributions increase with the eccentricity of the originating ganglion cells [14–16]. The smallest fibers are found in the PMB and originate from the perifoveal area where the packing densities of ganglion cells are highest. Therefore, axonal neural conduction speed increases from center to periphery, as confirmed by pattern VEP that showed an increase of the P100 implicit time with a small check-size (i.e., check edge: 15 minutes of visual arc) stimulation with respect to large check-size (i.e., check edge: 60 minutes of visual arc) [17–19].

## MfVEP responses in LHON disease

When comparing responses from LHON and control eyes, we found statistically significant differences of mean mfVEP P1 ITs and N1-P1 RADs at all five retinal eccentricities, obtained by the ring analysis (Table 3). This suggests a broad involvement of optic nerve axons derived not only from the central retina but also from the more peripheral retinal areas. Since our LHON eyes were assessed in the chronic phase (mean disease duration 32±8 months), our results are in agreement with all the observations regarding progression of retinal ganglion cells (RGCs) impairment in LHON. In fact, in the early stage of the disease, there is a selective involvement of the smaller-caliber fibers of the PMB, while in the chronic phase the neurodegenerative process expands to the remaining axons of the optic nerve leading to diffuse optic atrophy [17, 20–22].

Since we found that the differences between LHON and control eyes were statistically significant in all five rings, we considered that the ring analysis.is not an adequate method to determine the entity of the prevalent impairment that occurs in optic nerve fibers originating from different retinal areas. Therefore, in the mfVEP data analysis we considered studying the function describing the course of the mean P1 ITs and N1-P1 RADs with increased foveal eccentricities. As shown in Fig. 3a and b, we plotted the mean P1 ITs and N1-P1 RADs as a function of increasing retinal eccentricities, and analyzed the function of the linear and exponential fittings respectively. We found: 1) a different progression of the neural dysfunction in the cohort of LHON eyes when compared to controls at different retinal eccentricities, 2) that mean values of both mfVEP ITs and RADs of LHON eyes diverged extremely from the control values in the more central rings (0 to10 degrees from the fovea) compared to the more eccentric ones (10 to 20 degrees from the fovea), and 3) that the function describing the progression of mfVEP implicit time values, from central to more peripheral areas in our LHON patients, had a slope three times greater than controls.

Thus, by proposing the peculiar study of mfVEP IT function applied to the ring analysis data, we were able to detect a greater dysfunction of smaller axons driving responses from the central retina rather than larger axons driving responses from the more peripheral retina, confirming the greater involvement of the smaller axons of the PMB in LHON [17, 20, 23–26].

**Table 3** Mean values±1 standard deviation of mfVEP P1 implicit times (IT, ms) and response amplitude densities (RAD, nanovolt/degree$^2$) observed in control and Leber's hereditary optic neuropathy (LHON) eyes. The upper part of the table shows all eyes: the lower part divides the LHON eyes into groups "A" and "B" (see table footer)

| | R1: 0–2.5° | R2: 2.5–5° | R3: 5–10° | R4: 10–15° | R5: 15–20° |
|---|---|---|---|---|---|
| P1 Implicit time (ms) | | | | | |
| - Controls ($N$=22) | 104.78±4.76 | 98.65±4.28 | 92.64±6.54 | 90.05±5.68 | 86.44±7.78 |
| - LHON eyes ($N$=17) | 164.52±24.53 | 161.3±26.38 | 151.96±29.37 | 117.89±20.12 | 116.36±20.83 |
| - ANOVA f(1,38) | f=125.34; $p$<0.01* | f=120.90; $p$<0.01* | f=84.94; $p$<0.01* | f=38.44; $p$<0.01* | f=38.67; $p$<0.01* |
| N1-P1 RADs (ηVolt/deg$^2$) | | | | | |
| - Controls ($N$=22) | 33.78±7.76 | 15.65±3.28 | 5.72±2.24 | 4.26±1.28 | 3.24±1.58 |
| - LHON eyes ($N$=17) | 15.42±10.81 | 3.89±2.44 | 1.27±0.60 | 0.74±0.41 | 0.45±0.26 |
| - ANOVA f(1,38) | f=38.16; $p$<0.01* | f=152.78; $p$<0.01* | f=63.23; $p$<0.01* | f=118.51; $p$<0.01* | f=51.62; $p$<0.01* |
| P1 implicit time (ms) | | | | | |
| - LHON "A" eyes ($N$=8) | 150.8±20.9 | 148.2±21.1 | 131.7±20.1 | 103.3±11.3 | 99.4±13.4 |
| - LHON "B" eyes ($N$=9) | 176.8±21.5 | 173.0±26.0 | 169.9±24.5 | 130.9±17.1 | 131.4±13.0 |
| - ANOVA f(1,16) | f=6.36; $p$=0.0234 | f=4.59; $p$=0.0490 | f=12.2; $p$<0.01* | f=14.9; $p$<0.01* | f=24.9; $p$<0.01* |
| N1-P1 RADs (ηVolt/deg$^2$) | | | | | |
| - LHON "A" eyes ($N$=8) | 16.9±11.0 | 4.45±2.97 | 1.15±0.69 | 0.63±0.43 | 0.34±0.21 |
| - LHON "B" eyes ($N$=9) | 14.1±11.1 | 3.39±1.89 | 1.38±0.52 | 0.83±0.38 | 0.55±0.27 |
| - ANOVA f(1,16) | f=0.27; $p$=0.6117 | f=0.79; $p$=0.3872 | f=0.59; $p$=0.4515 | f=0.97; $p$ =0.3410 | f=3.28; $p$=0.0902 |

The ITs and RADs were derived from five concentric annular retinal regions (rings, R) centered on the fovea. We analyzed values deriving from 0 to 2.5 degrees (ring 1, R1), from 2.5 to 5 degrees (ring 2, R2), from 5 to 10 degrees (ring 3, R3), from 10 to 15 degrees (ring 4, R4), from 15 to 20 degrees (ring 5, R5). ANOVA= one way analysis of variance between groups. $N$ = number of eyes. "A" refers to the eyes with visual field spatial distribution of retinal sensitivity loss localized exclusively into 10 degrees, "B" refers to a loss extending over 10 degrees. * = statistically significant

This neurodegenerative process can be observed, though not exclusively, in the early stages of the LHON disease [17, 20], but remains more severe than the impairment of the neurons deriving responses from the more peripheral retinal areas, also in the advanced stagesof the disease. Several hypotheses may explain the size and eccentricity of axonal degeneration in LHON. The PMB, including the smallest fibers serving the central macula, have different cable properties due to their small size, and disproportionately consist of parvocellular RGCs which have peculiar morphological characteristics. Such anatomical and physiological properties may impose different vulnerabilities relating to defective bioenergetics, increased oxidative stress, abnormal mitochondrial dynamics, increased sensitivity to apoptosis, and possibly accumulation of damaged mitochondria [27]. Specifically considering various factors involving energetics and mitochondrial numbers, we proposed a mitochondrial stress index [24, 25]. The smallest axons have the highest rates of energy consumption to mitochondrial availability. As a consequence, the wave of degeneration seen in hystopathological and ultrastructural analyses matches the order of axonal fiber caliber in the human optic nerve [24, 25].

With regard to the relationship between the mfVEP abnormalities and the retinal sensitivity loss, we believe that the "ring analysis" does not make it possible to perform a correct statistical correlation between mfVEP data (ITs and RADs) and HFA MD and CPSD values. This comes from the observation that HFA and mfVEP data are obtained analyzing different topographical retinal areas. In fact, while the mfVEP responses are derived selectively from four concentric retinal areas, MD and CPSD values represent global indexes of the severity of the retinal sensitivity loss evaluated in 24 degrees [28]. Nevertheless, in LHON eyes we qualitatively examined the spatial distribution of the retinal sensitivity loss together with the impairment of the mfVEPs (see Table 1). The only consideration that we were able to make is that when the retinal sensitivity loss was located exclusively into the 10 central degrees (LHON eyes "A" in Table 1), we observed reduced abnormalities of mfVEP responses derived from the more external rings (R4 and R5), and this suggests a partial sparing of the neural conduction impairment along the more peripheral axons. Accordingly, in those LHON eyes whose retinal sensitivity loss was located not exclusively in the 10 degrees (LHON eyes "B" in Table 1), we observed a delay of the neural conduction along both smaller and bigger axons derived from central and mid-peripheral retinal areas respectively (more delayed mfVEP ITs in R1–R5 ring). All this is supported by the finding that mfVEP P1 ITs from more peripheral rings detected in LHON "B" eyes were significantly delayed with respect to LHON "A" eyes (Table 3).

In agreement with other published work [20], reduced RNFL thickness in our LHON were observed. It is worth noting that the mfVEP P1 IT delay of the axons of the optic nerve driving responses from within the more central areas (R1 and

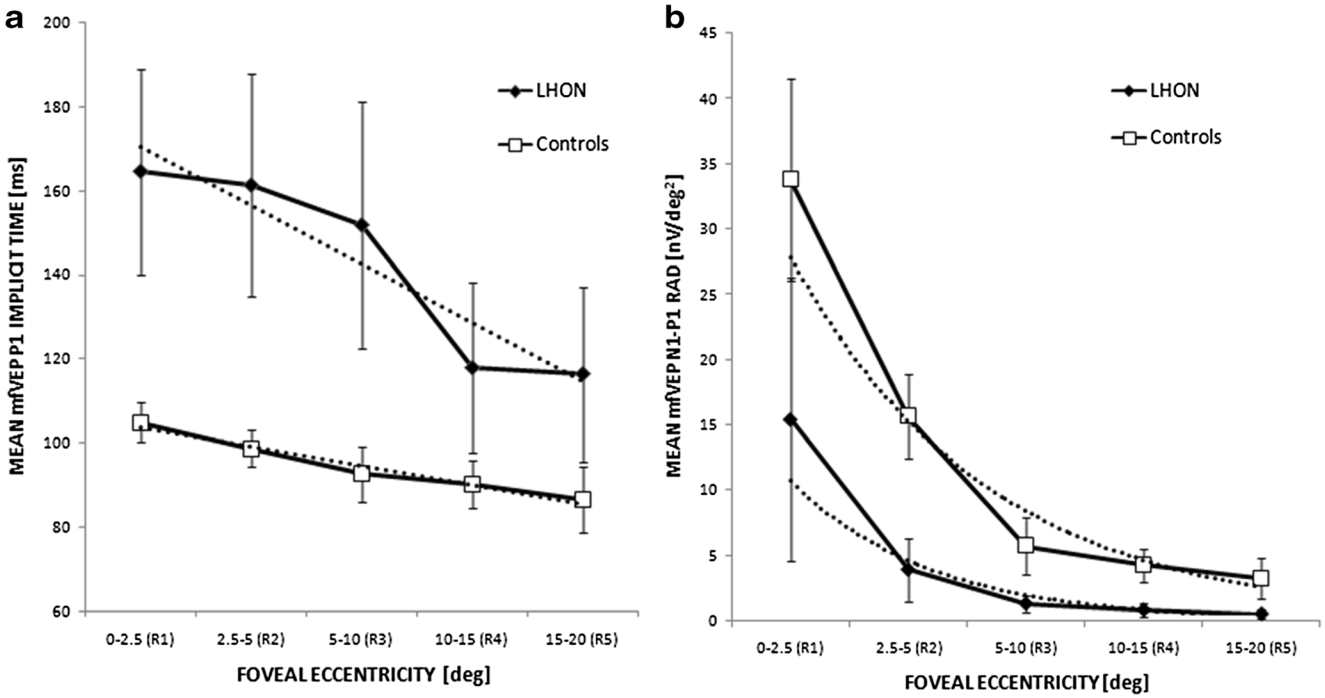


**Fig. 3** Multifocal visual evoked potentials (mfVEP) P1 implicit time (IT) (**a**) and N1-P1 response amplitude density (RAD) (**b**) mean values from controls and Leber's hereditary optic neuropathy (LHON) eyes plotted as a function of foveal eccentricities. R1 to R5 refer to ring analysis (see Methods). *Vertical bars* represent one standard deviation of the mean values. *Dashed lines* indicate the linear (LHON: $r=-0.95$; controls: $R=-0.98$) and exponential (LHON: $r^2=0.94$; controls: $r^2=0.93$) fittings for P1 ITs and N1-P1 RADs respectively. The relative functions show a progressive shortening of mfVEP P1 ITs and decrease of N1-P1 RADs in both controls and LHON eyes with increasing eccentricities (from R1 to R5), with a slope of the mean mfVEP P1 ITs function three times greater in LHON patients than in controls (LHON: $y=-13.33x+182.03$; controls: $y=-4.528x+108.1$), and a greater steepness proceeding from R3 to R4 (the center to periphery transitional retinal areas: 5 to 10 degrees of foveal eccentricity)

R2, corresponding to 0–2.5 and 2.5–5 degrees) was significantly correlated with the reduced RNFL thickness values measured in the temporal sector . This lead us to believe that the reported loss of the small fibers located in the temporal quadrant of the optic nerve and forming the papillo-macular bundle may induce a functional impairment detectable by this electrophysiological parameter (R1 and R2 mfVEP P1 IT). By contrast, we found not significant correlations between the R3–R5 (corresponding to 5 to 20 degrees) mfVEP P1 IT delay and N1-P1 RADs reduction and the thinning of the temporal and overall RNFL. This may be ascribed to the wide contribution to the overall OCT derived from the average thickness of fibers from all sectors including smaller and bigger axons. Alternatively, this masking effect may be due also to the type of mfVEP analysis used (ring analysis), and it is likely that a more adequate comparison may be obtained by using the mfVEP sector analysis, as was proposed in glaucoma [29]. However, this was not consistent with the main purpose of our study.

**Table 4** Correlations between P1 implicit time (IT) and N1-P1 response amplitude density (RADs) values of multifocal visual evoked potentials and retinal nerve fiber layer (RNFL) overall and temporal thickness values measured by optical coherence tomography (OCT) in Leber's hereditary optic neuropathy eyes

| | R1 | | R2 | | R3 | | R4 | | R5 | |
|---|---|---|---|---|---|---|---|---|---|---|
| | P1 IT | N1-P1 RADs | P1 IT | N1-P1 RADs | P1 IT | N1-P1 RADs | P1 IT | N1-P1 RADs | P1 IT | N1-P1 RADs |
| RNFL OCT overall thickness | $p=0.039$ | $p=0.704$ | $p=0.196$ | $p=0.935$ | $p=0.364$ | $p=0.467$ | $p=0.097$ | $p=0.252$ | $p=0.027$ | $p=0.185$ |
| | $r=-0.50$ | $r=-0.09$ | $r=-0.32$ | $r=0.02$ | $r=-0.23$ | $r=-0.18$ | $r=-0.41$ | $r=-0.29$ | $r=-0.53$ | $r=-0.33$ |
| RNFL OCT temporal thickness | $p=0.002$* | $p=0.398$ | $p=0.002$* | $p=0.983$ | $p=0.032$ | $p=0.494$ | $p=0.255$ | $p=0.958$ | $p=0.166$ | $p=0.233$ |
| | $r=-0.67$ | $r=-0.21$ | $r=-0.67$ | $r=0.005$ | $r=-0.52$ | $r=-0.17$ | $r=-0.29$ | $r=0.01$ | $r=-0.35$ | $r=-0.32$ |

R1–R5 refers to five concentric annular retinal regions (rings) centered on the fovea: R1: 0–2.5 degrees; R2: 2.5–5 degrees; R3:5–10 degrees; R4: 10–15 degrees; R5: 15–20 degrees. Pearson's test was used: an asterisk against a *p*-value indicates those which reached the significant level of 0.01

## Conclusions

In conclusion, the mfVEP ring analysis confirms that in LHON there is an axonal dysfunction involving both smaller and larger caliber fibers. It is worth noting that only once a study is conducted on the function of mfVEP ITs progression with increasing foveal eccentricities is it possible to differentiate the selective axonal population that suffers the greatest impairment. All this suggests that this peculiar study of mfVEP IT function may be an additional method, together with morphological (see RNFL OCT) and psychophysical (HFA) tests, for recognizing the more damaged site of the optic nerve injury.

**Acknowledgments** Research for this paper was financially supported partially by the Italian Ministry of Health (grant number: 2006 RF-FGB-2006-368547) and partially by Fondazione Roma. The authors acknowledge Dr. Valter Valli Fiore for technical help in electrophysiological evaluations.

**Conflict of interest** Each author states that he/she has no proprietary interest in the development or marketing of the instruments used in the present study, and no conflict of interest.

## References

1. Young B, Eggenberger E, Kaufman D (2012) Current electrophysiology in ophthalmology: a review. Curr Opin Ophthalmol 23:497–505
2. Hood DC, Greenstein VC (2003) Multifocal VEP and ganglion cell damage: applications and limitations for the study of glaucoma. Prog Retin Eye Res 22:201–251
3. Klistorner AI, Graham SL, Grigg JR, Billson FA (1998) Multifocal topographic visual evoked potential: improving objective detection of local visual field defects. Invest Ophthalmol Vis Sci 39:937–950
4. Parisi V, Ziccardi L, Stifano G, Montrone L, Gallinaro G, Falsini B (2010) Impact of regional retinal responses on cortical visually evoked responses: multifocal ERGs and VEPs in the retinitis pigmentosa model. Clin Neurophysiol 121:380–385
5. Baseler HA, Sutter EE, Klein SA, Carney T (1994) The topography of visual evoked response properties across the visual field. Electroencephalogr Clin Neurophysiol 90:65–81
6. Baseler HA, Sutter EE (1997) M and P components of the VEP and their visual field distribution. Vision Res 37:675–690
7. Park S, Park SH, Chang JH, Ohn YH (2011) Study for analysis of the multifocal visual evoked potential. Korean J Ophthalmol 25:334–340
8. Carelli V, Barboni P, Sadun AA (2006) Mitochondrial ophthalmology. In: DiMauro S, Hirano M, Shon EA (eds) Mitochondrial medicine. Informa Healthcare, London, pp 105–142
9. Carelli V, Ross-Cisneros FN, Sadun AA (2004) Mitochondrial dysfunction as a cause of optic neuropathies. Prog Retin Eye Res 23:53–89
10. Nikoskelainen EK (1994) Clinical picture of LHON. Clin Neurosci 2:115–120
11. Curcio CA, Allen KA (1990) Topography of ganglion cells in human retina. J Comp Neurol 300:5–25
12. Wassle H, Grunert U, Rohrenbeck J, Boycott BB (1990) Retinal ganglion cell density and cortical magnification factor in the primate. Vision Res 30:1897–1911
13. Sutter EE, Bearse MA (1999) The optic nerve head component of the human ERG. Vision Res 39:419–436
14. Fukuda Y, Watanabe M, Wakakuwa K, Sawai H, Morigiwa K (1988) Intraretinal axonsof ganglion cells in the Japanese monkey (Macaca fuscata): conduction velocity and diameter distribution. Neurosci Res 6:53–71
15. Ogden TE, Miller RF (1966) Studies of the optic nerve of the rhesus monkey: nerve fiber spectrum and physiological properties. Vision Res 6:485–506
16. Ogden TE (1984) Nerve fiber layer of the primate retina: morphometric analysis. Invest Ophthalmol Vis Sci 25:19–29
17. Ziccardi L, Sadun F, De Negri AM, Barboni P, Savini G, Borrelli E, La Morgia C, Carelli V, Parisi V (2013) Retinal function and neural conduction along the visual pathways in affected and unaffected carriers with Leber's hereditary optic neuropathy. Invest Ophthalmol Vis Sci 54:6893–6901
18. Kurita-Tashima S, Tobimatsu S, Nakayama-Hiromatsu M, Kato M (1991) Effect of the check size on the pattern reversal visual evoked potential. Electroencephalogr Clin Neurophysiol 80:161–166
19. Parisi V, Scarale ME, Balducci N, Fresina M, Campos EC (2010) Electrophysiological detection of delayed postretinal neural conduction in human amblyopia. Invest Ophthalmol Vis Sci 51:5041–5048
20. Barboni P, Carbonelli M, Savini G, Ramos Cdo V, Carta A, Berezovsky A, Salomao SR, Carelli V, Sadun AA (2010) Natural history of Leber's hereditary optic neuropathy: longitudinal analysis of the retinal nerve fiber layer by optical coherence tomography. Ophthalmology 117:623–627
21. Mashima Y, Imamura Y, Oguchi Y (1997) Dissociation of damage to spatial and luminance channels in early Leber's hereditary optic neuropathy manifested by the visual evoked potential. Eye (London) 11:707–712
22. Sharkawi E, Oleszczuk JD, Holder GE, Raina J (2012) Clinical and electrophysiological recovery in Leber hereditary optic neuropathy with G3460A mutation. Doc Ophthalmol 125:71–74
23. Sadun AA, Win PH, Ross-Cisneros FN, Walker S, Carelli V (2000) Leber's hereditary optic neuropathy differentially affects smaller axons in the optic nerve. Trans Am Ophthalmol Soc 98:223–232
24. Pan BX, Ross-Cisneros FN, Carelli V, Rue KS, Salomao SR, Moraes-Filho MN, Moraes MN, Berezovsky A, Belfort R Jr, Sadun AA (2012) Mathematically modeling the involvement of axons in Leber's hereditary optic neuropathy. Invest Ophthalmol Vis Sci 53:7608–7617
25. Sadun AA, La Morgia C, Carelli V (2013) Mitochondrial optic neuropathies: our travels from bench to bedside and back again. Clin Experiment Ophthalmol 41:702–712
26. Sadun AA (1998) Acquired mitochondrial impairment as a cause of optic nerve disease. Trans Am Ophthalmol Soc 46:881–923
27. Procaccio V, Bris C, Chao de la Barca JM, Oca F, Chevrollier A, Amati-Bonneau P, Bonneau D, Reynier P (2014) Perspective of drug-based neuroprotection targeting mitochondria. Rev Neurol (Paris) 170:390–400
28. Lachenmayr BJ, Vivell PMO (1993) Principles of perimetry. In: Lachenmayr BJ, Vivell PMO (eds) Perimetry and its clinical correlation. Thieme Medical Publishers Inc., New York, pp 12–13
29. Moschos MM, Georgopoulos G, Chatziralli IP, Koutsandrea C (2012) Multifocal VEP and OCT findings in patients with primary open angle glaucoma: a cross-sectional study. BMC Ophthalmol 12:34